HHS Public Access

Author manuscript

*J Bone Miner Res*. Author manuscript; available in PMC 2020 July 13.

Published in final edited form as:

*J Bone Miner Res*. 2020 June ; 35(6): 1119–1131. doi:10.1002/jbmr.3978.

# Targeted Reduction of Senescent Cell Burden Alleviates Focal Radiotherapy-Related Bone Loss

**Abhishek Chandra**[1,2,3], **Anthony B Lagnado**[1,3], **Joshua N Farr**[3,4], **David G Monroe**[3,4], **Sean Park**[5], **Christine Hachfeld**[3], **Tamar Tchkonia**[3], **James L Kirkland**[1,2,3], **Sundeep Khosla**[3,4], **João F Passos**[1,2,3], **Robert J Pignolo**[1,2,3,4]

[1]Department of Physiology and Biomedical Engineering, Mayo Clinic College of Medicine, Rochester, MN, USA

[2]Department of Medicine, Division of Geriatric Medicine and Gerontology, Mayo Clinic College of Medicine, Rochester, MN, USA

[3]Robert and Arlene Kogod Center on Aging, Mayo Clinic College of Medicine, Rochester, MN, USA

[4]Division of Endocrinology, Department of Medicine, Mayo Clinic College of Medicine, Rochester, MN, USA

[5]Department of Radiation Oncology, Mayo Clinic College of Medicine, Rochester, MN, USA

## Abstract

Clinical radiotherapy treats life-threatening cancers, but the radiation often affects neighboring normal tissues including bone. Acute effects of ionizing radiation include oxidative stress, DNA damage, and cellular apoptosis. We show in this study that a large proportion of bone marrow cells, osteoblasts, and matrix-embedded osteocytes recover from these insults only to attain a senescent profile. Bone analyses of senescence-associated genes, senescence-associated beta-galactosidase (SA-β-gal) activity, and presence of telomere dysfunction-induced foci (TIF) at 1, 7, 14, 21, and 42 days post–focal radiation treatment (FRT) in C57BL/6 male mice confirmed the development of senescent cells and the senescence-associated secretory phenotype (SASP). Accumulation of senescent cells and SASP markers were correlated with a significant reduction in bone architecture at 42 days post-FRT. To test if senolytic drugs, which clear senescent cells, alleviate FRT-related bone damage, we administered the senolytic agents, dasatinib (D), quercetin (Q), fisetin (F), and a cocktail of D and Q (D+Q). We found moderate alleviation of radiation-induced bone damage with D and Q as stand-alone compounds, but no such improvement was

Address correspondence to: Abhishek Chandra, PhD. E-mail: chandra.abhishek1@mayo.edu Or Robert J. Pignolo, MD, PhD, Department of Physiology and Biomedical Engineering and Department of Medicine, Division of Geriatric Medicine & Gerontology, Mayo Clinic College of Medicine, 200 First Street SW Rochester, MN 55905, USA., pignolo.robert@mayo.edu.

Authors' roles: AC and RJP designed the study. AC, AL, JNF, and CH performed the experiments. AC, DM, SP, SK, JP, and RJP analyzed and interpreted the data. AC and RJP wrote the manuscript and all authors revised and approved the final version of the manuscript.

Disclosures

JLK and TT have a financial interest related to this research. Patents on senolytic drugs are held by Mayo Clinic. This research has been reviewed by the Mayo Clinic Conflict of Interest Review Board and was conducted in compliance with Mayo Clinic

Conflict of Interest policies. No conflicts of interest, financial or otherwise, are declared by the other authors.

Additional Supporting Information may be found in the online version of this article.

seen with F. However, the senolytic cocktail of D+Q reduced senescent cell burden as assessed by $TIF^{+}$ osteoblasts and osteocytes, markers of senescence (*p16*$^{Ink4a}$ and *p21*), and key SASP factors, resulting in significant recovery in the bone architecture of radiated femurs. In summary, this study provides proof of concept that senescent cells play a role in radiotherapy-associated bone damage, and that reduction in senescent cell burden by senolytic agents is a potential therapeutic option for alleviating radiotherapy-related bone deterioration.

**Keywords**

OSTEOPOROSIS; RADIOTHERAPY; SENESCENCE; SENOLYTICS; TELOMERE DYSFUNCTION

## Introduction

Cellular senescence is a key mechanism underlying several age- and disease-related comorbidities and is generally defined as the static condition of a cell in which survival pathways induce resistance against apoptotic triggers.[1] Oxidative stress, oncogenes, DNA damage, genomic instability, telomere shortening, and alteration of proteostasis are a few of the physiological inducers of cellular senescence.[2] One of the characteristics of cellular senescence is the impairment of telomeres, structures that cap the ends of chromosomes that consist of TTAGGG repeats associated with several telomere-binding proteins collectively known as the shelterin complex.[3] During replicative senescence, telomeric ends lose their telomere-loop (t-loop) configuration, a process known as “uncapping”, and become associated with various DNA damage response proteins, a phenomenon characterized by telomere dysfunction-induced foci (TIF).[3] Additionally, exposure to high doses of radiation has been shown to induce double-stranded breaks at telomere regions, inducing a DNA damage response (DDR) that remains persistent for long periods of time both in vitro and in vivo.[3–5]

Aging may reduce the capacity of the immune system to clear senescent cells.[6] Senescent cells can reside in tissues for an extended time, as well as have local and distant effects through their release of a pro-inflammatory and deleterious secretome referred as the senescence associated secretory phenotype (SASP). Senescence and the SASP have now been established as contributors to age-related frailty and other disorders.[7]

Osteoporosis is common in old age and is accompanied by a high risk for fracture.[8] Our recent report of elevated expression of cyclin-dependent kinase inhibitors (CDKi) *p16*$^{Ink4a}$ and *p21* in aged bone cells[9] suggests that cellular senescence plays a role in the pathophysiology of osteoporosis. Cellular senescence is also associated with altered expression of SASP factors in bone, with an increase in pro-inflammatory factors. Moreover, clearance of senescent cells using genetic and pharmaceutical interventions improves bone quality in aged mice.[10]

Radiation has been used to induce senescent cells in vitro by generating oxidative stress, DNA double-strand and single-strand breaks, and chromatin disruption.[11] However, effects of radiation on bone are multifaceted and are largely dose-dependent, which can only be

studied in vivo. Both low-dose and high-dose radiation treatment regimens result in bone loss, mainly due to increase in osteoclast function,[12] and increases in DNA damage and cellular apoptosis of the bone lineage cells.[13,14] Several studies suggest that bone marrow cells of the hematopoietic lineage are the most sensitive to radiation damage.[15–17] Cells that are responsible for maintaining bone homeostasis, such as osteoblasts, osteocytes, and mesenchymal stem cells (MSCs), undergo varying degrees of DNA damage and apoptosis, with osteoblasts being more sensitive and MSCs more resistant. Thus, it is unclear whether cells that escape the initial insults of acute radiation in vivo are functional or become senescent. Here we studied the impact of accumulation of senescent osteoblasts and osteocytes on bone architecture post–focal radiation treatment (FRT) and whether clearance of senescent cells using senolytic agents could alleviate the deterioration in bone quality seen with radiation treatment.[18]

## Materials and Methods

### Animal studies

All animal studies were approved by the Institutional Animal Care and Use Committee at Mayo Clinic. C57BL/6 male mice were purchased from The Jackson Laboratory (Bar Harbor, ME, USA) and housed in our facility at 23°C to 25°C with a 12-hour light/dark cycle and were fed with standard laboratory chow (PicoLab® Rodent Diet 20 #5053; LabDiet, St. Louis, MO, USA) with free access to water. Col2-Cre Rosa-Tomato (Col2/Tomato) mice were generated by breeding Col2-Cre mice and Rosa-Tomato mice obtained from The Jackson Laboratory and as described.[14] Mice received a dose of FRT comparable to that received by patients suffering from spinal metastases, which is a single dose of 24 Gy on day 0. This dose is used as a proof of concept and an attempt to mimic patients with oligometastatic cancers to spine (mostly prostate and lung primary), who are treated aggressively with stereotactic body radiation therapy (SBRT) at our institution. Because these oligometastatic patients have the potential to have longer term survival (>1 to 3 years), it is highly relevant to study bystander effects to the normal bone (ie, SBRT treatment toxicities), using femur as a simplistic model of choice, with the goal of improving normal tissue complications in a tumor adjacent bone. Using X-Rad-SmART (Precision X-Ray Inc. [PXi], North Branford, CT, USA) an image-guided focal dose of 24 Gy at 6.6 Gy/min was delivered to a 5-mm region of the distal metaphyseal region of the right femur, while the left femur served as the contralateral control. Radiated (R) and nonradiated (NR) femurs were harvested on days 1, 7, 14, 21, and 42 (a minimum of $n = 3$ animals/time point) for gene expression analyses and at 42 days post-FRT for measurements of bone architecture. Dasatinib (D; 5 mg/kg, $n = 5$) (LC Laboratories, Woburn, MA, USA), quercetin (Q; 50 mg/kg, $n = 5$) (Cayman Chemical Company INC, Ann Arbor, Michigan, USA), fisetin (F; 50 mg/kg, $n = 5$) (Sigma-Aldrich Corp., St. Louis, MO, USA), or a cocktail of D and Q (D 5 mg/kg + Q 50 mg/kg, $n = 5$)[11,19] were administered on day 0 and on day 14 post-FRT by oral gavage, with vehicle ($n = 5$) being the control. Animals were injected with Alizarin-3-methyliminodiacetic acid (Sigma-Aldrich Corp.) and calcein (Sigma-Aldrich Corp.), 9 and 2 days before tissue harvest, respectively. Body weight of the animals did not change before or after FRT or treatment (data not shown). Serum was collected at time of death to determine N-terminal propeptide of Collagen alpha-1 (I) chain (P1NP) (G-Bioscienses™ IT5184, St.

Louis, MO, U.S. A.) and Collagen C-Terminal Telopeptide (CTX-I) (LS Bio, Seattle, WA, USA) levels by enzyme-linked immuno sorbent assay (ELISA) as per manufacturer's instructions. One animal from the D group was removed from the study because of severe fight wounds and weight loss. All animal studies were performed in a double-blinded manner, with the animals being coded by a unique identifier.

### Methyl methacrylate tissue embedding and histology

R and NR femurs were processed at day 42 post-FRT for methyl methacrylate (MMA) embedding. Nondecalcified femurs were sectioned into 5-μm sections that were used for static histomorphometry and TIF assay, while 8-μm sections were used for dynamic histomorphometry.

### Micro–computed tomography analysis

Bones were harvested 42 days post-FRT and scanned by high-resolution micro–computed tomography (μCT) (vivaCT 40; Scanco Medical AG, Brüttisellen, Switzerland). Images were scanned from the distal end of the femur, corresponding to a 1-mm to 5-mm area above the growth plate. All images were first smoothed by a Gaussian filter (sigma = 1.2, support = 2.0), then thresholded corresponding to 30% of the maximum available grayscale values as described.[14,20] We used a visual confirmation to create this global threshold and one that includes most of the bone architecture, a method described in detail.[20] Volumetric bone mineral density (vBMD), bone volume fraction (BV/TV), trabecular thickness (Tb.Th), trabecular separation (Tb. Sp), trabecular number (Tb.N), and structure-model index (SMI) were calculated using 3D standard microstructural analysis.

### SA-β-galactosidase staining

SA-β-galactosidase (SA-β-gal) is a marker to identify senescent cells.[11] The SA-β-gal assay was performed on bone sections ($n$ = 4 per group) at 28 days postradiation using a standard staining kit (Cell Signaling Technology, Beverly, MA, USA; Catalog# 9860S). Briefly, frozen bone sections were air dried, washed in PBS before and after fixation, and incubated with the β-gal staining solution containing the substrate X-gal as per the manufacturer's instructions. The slides were incubated at 37°C in a non-$CO_2$ chamber for 16 to 20 hours. Slides were visualized using a Nikon Eclipse CiL Microscope (Nikon, Tokyo, Japan) at a resolution of 200×. Blue stained SA-β-gal+ cells on the bone surface were quantified per mm of bone surface.

### TIF assay

TIF assay ($n$ = 4/group) was performed on deplasticized-MMA embedded bone sections by incubation in 0.01M citrate buffer (pH 6.0) at 95°C for 15 min then on ice for 15 min before washing in water and PBS for 5 min each. The TIF assay was performed as described.[3] In-depth Z-stacking was used (a minimum of 135 optical slices with ×63 objective). The number of TIFs per cell was assessed by manual quantification of partially or fully overlapping (in the same optical slice, Z) signals from the telomere probe (Cy-3-labelled telomere-specific (CCCTAA) peptide nucleic acid probe (F1002, Panagene) 54, Techno 10-ro, Yuesong-gu, Daejeon 34027, South Korea) and γ-H2AX, phosphorylation of the C-

terminal end of histone H2A.X, a marker for double strand breaks in DNA (Cell Signaling Technology, Danvers, MA, USA). In z-by-z analysis. Images were deconvolved using a deconvolution algorithm, with blinded deconvolution in AutoQuant X3 (Media Cybernetics, Rockville, MD, USA). We defined a minimum of two TIFs to assign it as a $TIF^+$ cell. $TIF^+$ osteoblasts (~50 to 100 per bone section/animal), $TIF^+$ osteocytes (~35 to 50 per bone section/animal), and $TIF^+$ bone marrow cells (~1000 per bone section/animal) were quantified using FIJI (an Image J distribution software; NIH, Bethesda, MD, USA; https://imagej.nih.gov/ij/).[21]

## TUNEL assay

Four-month-old Col2-Cre-Td+Tomato male mice received radiation (24 Gy) in a 5-mm region of the right femoral metaphysis, accompanied with intermittent treatments on day 0 and 14, with either vehicle ($n = 4$ mice) or D+Q ($n = 4$ mice); bones were collected on day 42 post-FRT and processed for frozen sectioning. The TUNEL assay was carried out according to the manufacturer's instructions (ApopTag Fluorescein In Situ Detection Kit; EMD Millipore, Billerica, MA, USA) and as described.[14,22]

## Isolation of bone cells

Bone cells were isolated for mRNA analysis as described.[9] Briefly, flushed bone marrow cells were pooled and treated with red blood cell (RBC) lysis buffer solution (eBioscience, San Diego, CA, USA) for 5 min at room temperature. Following a brief centrifugation and resuspension in FACS buffer, the resulting bone marrow mononuclear cells (BMMNCs) were further processed using magnetic activated cell sorting (MACS; autoMACS-Pro magnetic cell sorter; Miltenyi Biotec, Inc., San Diego, CA, USA) to obtain highly enriched fractions of myeloid cells, osteoblasts, and osteocytes, as described.[9]

## qRT-PCR

A 5-mm region below the growth plate of the distal metaphyseal femur was cut out from the R and NR legs. After removal of muscle tissue, the bone samples were homogenized and total RNA was isolated using RNeasy Mini Columns (QIAGEN, Valencia, CA, USA). mRNA extraction from enriched myeloid cells, osteoblasts, and osteocytes from young (6 months old) and old (24 months old mice) was performed as described.[9] cDNA was generated from mRNA using the High-Capacity cDNA Reverse Transcription Kit (Applied Biosystems by Life Technologies, Foster City, CA, USA) according to the manufacturer's instructions and RT-qPCR was performed as described in our previous studies.[9] All primer sequences were obtained from Dr. Khosla's laboratory and have been authenticated by previous studies.[9,10] Primers were designed so that they overlapped two exons. A detailed list of primer sequences are provided in Supplementary Table S1.

## Static and dynamic histomorphometry

Static histomorphometry was performed on Goldner's trichrome–stained sections, counting osteoblast numbers (N. Ob) per mm of bone surface. Dynamic histomorphometry was performed on unstained deplasticized sections and mineralizing surface (MS/BS) and bone formation rate (BFR) were calculated as described.[23] Both static and dynamic

histomorphometry were performed using the OsteoMeasure Histomorphometry System (OsteoMetrics, Inc., Decatur, GA, USA) with an Olympus Dotslide motorized microscope system (Olympus, Waltham, MA, USA).

### Statistical power, sample size, and computational analyses

Based on prior studies, and with 5 mice/group, we estimated 80% power to detect a 30% decrease in BV/TV in the R-treated bone as compared to NR bone, assuming two-sided alpha of 5% (effect size of 0.5, paired *t* test using nQuery Advisor 7.0; Statsols, Boston, MA, USA). With 5 mice/group, there would be 80% power to detect a 1-standard deviation (SD) change (effect size = 1) in bone parameters between the two independent groups of mice (R-Veh versus R-Senolytic-treated group), assuming two-sided alpha of 5% (two-sample *t* test using nQuery Advisor 7.0). For histology and mRNA analysis with a minimum of three mice/group, we have previously achieved a 30% change (assuming a two-sided alpha of 5%). The proposed analysis and sample size calculation were facilitated by the biostatistics core at the Mayo Clinic. All statistics were performed using GraphPad Prism 8.1.1 software (GraphPad Software, Inc., La Jolla, CA, USA). Data are expressed as medians with interquartile range and analyzed by two-tailed paired *t* tests where the factors were: radiation (R versus NR-contralateral control leg in the same animal) and by two-way analysis of variance (ANOVA) followed by a Tukey post hoc analysis where variables were radiation (NR versus R) and drug treatment (D+Q-treated versus vehicle-treated). Heat maps were created using Morpheus software (https://software.broadinstitute.org/morpheus).

## Results

### Association of accumulated senescent osteoblasts and osteocytes with bone damage postradiation

In order to ascertain the role of cellular senescence as a cause of radiotherapy-related bone deterioration, we exposed an area of 5 mm in the femoral metaphysis to a single dose of 24 Gy radiation, and analyzed the bones at different time points. We were able to confirm our previous reports and saw a significant bone loss 4 weeks post-FRT (Fig. 1A,B).[14,22] To confirm the presence of senescent cells 28 days post-FRT, we stained for SA-β-gal activity in both NR and R femurs, and found a significant 4.4-fold increase in the SA-β-gal$^+$ cells on the bone surface in the R femurs (Fig. 1C,D). We also detected a 4.7-fold increase in TIF$^+$ osteocytes (Fig. 1E,F) and a 3.7-fold increase in TIF$^+$ bone lining cells including osteoblasts (Fig. 1G,H) in R femurs at 42 days post-FRT.

### FRT increases expression of senescence and SASP related genes

In order to understand the dynamics of senescence markers, we determined the gene expression levels of *p16$^{Ink4a}$* and *p21* on days 1, 7, 14, 21, and 42 post-FRT. Both *p16$^{Ink4a}$* and *p21* had significantly higher expression at all time points in R femurs compared to NR femurs (Fig. 2A,B). Interestingly, *p21* expression increased dramatically by 12.8-fold on day 1, followed by a gradual reduction to 8.8-fold on day 7, 4.3-fold on day 14, 3.6-fold on day 21, and finally 2.7-fold on day 42 post-FRT (Fig. 2A). Conversely, *p16$^{Ink4a}$* increased by 3.4-fold on day 1, and thereafter maintained significantly higher gene expression in the R femurs at all time points post-FRT (4.4-fold on day 7, 1.8-fold on day 14, and 2.7-fold on

day 21), reaching the highest expression level with a 11.7-fold increase on day 42 post-FRT (Fig. 2B). As shown by heat maps, apart from *p16*$^{Ink4a}$ and *p21*, significant increases in the expression of the other CDKi markers, *p15*$^{Ink4b}$ and *p27*$^{Kip1}$, were also observed in R bone at 14 days post-FRT, while *p19*$^{Ink4d}$ remained essentially unchanged (Fig. 2C). Whole-bone gene expression patterns in *p16*$^{Ink4a}$ and *p21* were also similar to changes in bone cells from aged mice at 14 days post-FRT (Supplementary Fig. S1). This trend of increased expression of cell cycle inhibitors was also observed at 21 days post-FRT, with significant increases in *p16*$^{Ink4a}$, *p21*, *p15*$^{Ink4b}$, and *p27*$^{Kip}$ (Fig. 2D; Supplementary Fig. S1).

Because we did not see changes in bone architecture until day 14 post-FRT, we evaluated gene expression of the SASP factors at 2 weeks to understand the earliest change in bone environment triggering the bone loss. Based on previously described SASP factors in different model of induction of senescence including X-rays,[9,24–26] we analyzed 46 SASP genes using qRT-PCR, out of which 18 were markedly elevated 14 days post-FRT (Fig. 3A), and a select few were downregulated. Out of 18 genes that were significantly upregulated post-FRT, 10 genes (*Ccl2*, *Ccl3*, *Ccl5*, *Ccl7*, *Ccl8*, *Cxcl1*, *Cxcl2*, *Icam1*, *Igfbp4*, and *Mmp12*) were a subset of those 22 that were significantly upregulated in aged bone cells as well (Fig. 3B and as published in Farr and colleagues[9]). *Mmp12* was one of the most upregulated genes, with a 12-fold increase post-FRT in the R femur, which correlated well with the individual expression levels in aged myeloid and osteocyte fractions (Fig. 3B and as published in Farr and colleagues[9]). Both *Icam1* and *Igfbp4* had modest, but highly significant 1.6-fold and 1.4-fold increases post-FRT, respectively (Fig. 3C), which were also associated with expression levels seen in aged myeloid and osteocyte populations. Among the interleukins, *Il1a*, *Il1b*, and *Il11* were significantly downregulated post-FRT, while *Il10* and *Il18* underwent 1.5-fold and 2.7-fold increases, respectively (Fig. 3D). In search for SASP factors that were specific for radiation as an inducer of senescence, we expanded the list of chemokines tested and found that several of them were upregulated post-FRT, among which *Cxcl1*, *Cxcl2*, *Cxcl9*, *Cxcl16*, *Ccl1*, *Ccl2*, *Ccl4*, *Ccl5*, and *Ccl7* were significant, while *Cxcl10*, *Ccl3*, and *Ccl8* showed a trend toward increases (Fig. 3E). *Cxcl5* and *Ccl11* were two of the chemokines that were significantly downregulated (Fig. 3E).

## Selective efficacy of senolytic drugs in alleviating FRT-related bone damage

The accumulation of senescent cells and consequent expression of SASP markers post-FRT were associated with a 28.3% reduction in BV/TV at day 42, together with significant changes in trabecular number (Tb.N, −14.8%), trabecular separation (Tb.Sp, 13.97%), trabecular thickness (Tb.Th, −4.11%), and BMD (−17.35%) (Fig. 4A). Targeted clearance of senescent cells has been shown to improve health span[19] and also alleviate age-related osteoporosis.[10] Therefore, we tested the efficacy of three senolytic regimens, including D, Q, and F, where the treatments were given on days 0 and 14 post-FRT and the bones were analyzed at 42 days post-FRT. Intriguingly, none of the senolytic compounds singly were able to completely rescue the phenotype and failed to reach significance in any bone parameter measured, including BV/TV (D, 35.8%, n.s. [not significant]; Q, 34.5%, n.s.; and F, 9.52%, n.s.), connectivity density (Conn.Dens.) (D, 45.05%, $p = .051$; Q, 47.61%, n.s.; and F, 43.60%, n.s.), structural model index (SMI) (D, −14.38%, n.s.; Q, −14.19%, n.s.; and F, −9.57%, n.s.), and Tb.Th (D, 8.02%, n.s.; F, −6.76%, n.s.; and Q, 5.22%, n.s.), compared

to vehicle-treated R femurs (Fig. 4A,B and data not shown). Because the stand alone senolytic regimen did not work as we expected, we decided to test the senolytic cocktail of D+Q. Intriguingly, the senolytic cocktail of D+Q resulted in significant improvements in the radiated bones, with increase in BV/TV (74.2%, $p = .0046$), increase in the Conn.Dens. (91.29%, $p = .018$), a nonsignificant decrease in SMI (−24.19%, n.s.), and a nonsignificant increase in Tb.Th (12.88%, $p = .096$) compared to the vehicle R femurs (Fig. 4C,D).

## Senolytic cocktail of D+Q preserves bone formation postradiation

Looking within the femoral metaphysis (Fig. 5A), vehicle-treated NR femurs had visible bone lining cells including osteoblasts, while the Veh-R femurs had significantly reduced numbers of bone lining cells. Using static histomorphometry in Goldner's Trichrome–stained nondecalcified tissue sections (Fig. 5B), we confirmed a 46.3% reduction in osteoblast numbers per bone perimeter (N.Ob/B.Pm), fivefold increase in adipocyte numbers per total area (N.Ad/T.Ar), and 35.4% decrease in osteocyte number per bone area (N.Ot/B.Ar) post-FRT. D+Q treatment resulted in a significant 66% increase in N.Ob/B.Pm, a fourfold decrease in N.Ad/T.Ar, and a nonsignificant 25.6% increase in N.Ot/B.Ar compared to vehicle-treated R bones (Fig. 5C). Double labeling with Alizarin and Calcein 9 and 2 days before tissue harvest, respectively, demonstrated a 73.3% reduction in MS/BS and an approximately 93.3% decrease in bone formation rate per bone surface (BFR/BS) in vehicle-treated R femurs (Fig. 6A,B). In D+Q-treated R femurs, a 1.95-fold increase in MS/BS and a 4.5-fold increase in BFR/BS were observed when compared to vehicle treated R bones (Fig. 6A,B). These changes in mineralizing ability of cells were not reflected in the gene expression profiles of bone marker genes, *Runx2* and *Bglap* (Osteocalcin), in which no significant changes were observed in either of the groups (Supplementary Fig. S2). Interestingly, the bone formation marker N-terminal propeptide of type I procollagen (P1NP) in the serum, was significantly elevated in D+Q-treated mice as compared to the vehicle-treated mice (Fig. 6C), but no change in the resorption marker, serum C-terminal telopeptide of type I collagen (CTX), was observed post-D+Q treatment (Supplementary Fig. S3).

## Targeted reduction of senescent cell burden and SASP by senolytic treatment postradiotherapy

In order to assess the mechanisms underlying almost complete suppression of bone formation 42 days post-FRT, we first tested whether osteoblasts on the bone surface were undergoing apoptosis. As reported,[13,14,22] high-dose FRT resulted in osteoblast apoptosis, but the overall percentage of osteoblasts undergoing apoptosis was less than 10% (Supplementary Fig. S4A,B). D+Q had no effect on cell survival of the radiated osteoblasts, and the R femurs had a nonsignificant increase in apoptotic osteoblasts as compared to the NR femurs (Supplementary Fig. 4A,B). Examining the senescence profile in bone tissue from untreated and D+Q-treated animals at 42 days post-FRT, we observed that D+Q significantly suppressed *p21* and $p16^{Ink4a}$ gene expression (Fig. 7A,B). As shown in Fig. 1, FRT led to an increase of $TIF^+$ senescent osteocytes and $TIF^+$ senescent bone lining cells including osteoblasts. Strikingly, intermittent (and infrequent) dosing of D+Q reduced $TIF^+$ senescent osteocytes (Fig. 7C,D), $TIF^+$ senescent bone lining cells including osteoblasts (Fig. 7E,F), and $TIF^+$ senescent bone marrow cells (Fig. 7G) to levels found in NR femurs.

We further showed that reduction of senescent cell burden by D+Q was able to suppress expression of several SASP genes 42 days post-FRT, including *Ccl-2*, *Ccl-4*, *Ccl-5*, *Ccl-7*, *Cxcl-1*, *Cxcl-9*, *Cxcl-13*, *Cxcl-16*, *Cxcr5*, *Il10*, *Il18*, and *Mmp2* (Fig. 8).

## Discussion

The goal of this study was to establish senescence as one of the key mechanisms behind the pathophysiology of radiotherapy-related osteoporosis. To our knowledge, this is the first study showing early and late senescence responses, upregulation of *p21* and $p16^{Ink4a}$, respectively, and the presence of senescent cells (osteoblasts and osteocytes) in the focally radiated bone microenvironment. Furthermore, this study delineates the differential efficacy of senolytic drugs in alleviating radiotherapy-related bone damage, with the senolytic cocktail of D+Q being the most effective. Our study also gives the first direct evidence that accumulation of senescent osteoblasts and osteocytes markedly reduces bone formation rate, which is restored upon short-term episodic treatment with D+Q. Furthermore, reduction of senescent cell burden by D+Q was accompanied by suppression of *p21* and $p16^{Ink4a}$ gene expression and that of the pro-inflammatory SASP.

Effects of radiation on bone damage have been studied extensively,[14,22,27] but a detailed mechanism for the extent of bone loss has not been elucidated. Low-dose radiation can cause local and distal bone loss, possibly by increased osteoclast activity.[12,28] However, osteoclast number or activity decreases with high-dose limited-field radiation preceded by a transient increase,[14,29] and it has been reported that alendronate fails to rescue bones exposed to high-dose limited-field radiation.[13] It has also been shown that high-dose ionizing radiation negatively affects osteoclast formation in vitro.[30,31] Although we were not able to assess the role of bone resorption due to osteoclast activity, we believe that the differences in bone volume in the NR and R bone, 28 and 42 days post-FRT, are due to complete suppression in bone mineralization which resulted in lack of accrual of new bone in the R bones. Future studies may help assess the transient activation of osteoclasts during single high and multiple-fractionated doses of radiotherapy.

Exploring alternative mechanisms, we showed that high-dose focal radiation causes DNA damage, osteoblast and osteocyte apoptosis, and fate conversion of MSCs into adipocytes.[14,22] Although 10% to 12% of osteoblasts and 35% of osteocytes sustain DNA damage, only one-half of them undergo apoptosis.[14] This, however, did not explain the near complete suppression of bone formation rate in radiated bone.[14] Here we tested the hypothesis that bone-forming cells, which survive radiation-induced DNA, damage (ie, apoptosis-resistant cells), become senescent and result in dysfunctional osteoblasts and osteocytes. As a confirmation of this hypothesis, we showed here that less than 10% osteoblasts on the vehicle-treated radiated bone surface were apoptotic by day 42 (Supplementary Fig. 4), and ~40% of bone lining cells including osteoblasts were senescent (Fig. 1G,H).

Radiation has been used to generate senescence in cell culture models, and radiation damage to telomeres result in TIFs.[3,32] Moreover, the overall DDR peaks at day 1 postradiation and then subsides, but the accumulation of DNA damage at telomere ends remains consistent

over a period of time.[3] We detected senescence in radiated femurs by three different methods, including SA-β-gal staining, detection of $TIF^+$ cells, and gene expression of senescence markers and the SASP. To our knowledge, detection of senescent osteoblasts and osteocytes in nondecalcified bone tissue using the TIF assay also represents a technological advancement.

We compared markers of senescence and the SASP in radiated bone with aged bone cells. This was performed in order to better understand the mechanistic similarities and differences in the induction of cell senescence and to delineate changes due to acute DNA damage caused by radiation versus the more gradual accumulation of senescent cells that occurs with age. As shown previously,[9] both *p21* and $p16^{Ink4a}$ are expressed in bone cells of aged mice, but $p16^{Ink4a}$ expression was significantly higher, suggesting perhaps a greater role of $p16^{Ink4a}$ in age-related cellular senescence. As compared to aging, similar changes in both *p21* and $p16^{Ink4a}$ were observed with radiation. However, although $p16^{Ink4a}$ expression levels exhibited an upward trend with increasing time post-FRT, *p21* expression was highest on day 1 post-FRT and reduced thereafter. Our data do not clarify which cell types undergo senescence through *p21* expression or $p16^{Ink4a}$ expression exclusively, or whether the same cell(s) express both *p21* and $p16^{Ink4a}$. However, our previous data suggest that *p21* and $p16^{Ink4a}$ may be expressed differentially in specific bone cells.[9] Furthermore, the time course of *p21* and $p16^{Ink4a}$ expression after FRT strongly supports the rationale for timing of senolytic dosing with clinic correlates.

Most reports on senescence in bone postradiation have been limited to hematopoietic lineage cells,[33,34] and the role of senescent osteoblasts and osteocytes in affecting bone formation has not been previously studied. Senescent osteoblasts fail to carry out mineralization, whereas senescent osteocytes with an altered SASP profile may also affect bone quality. The presence of senescent cells is detrimental for tissue regeneration,[7] and their clearance by the use of senolytic drugs likely decreases senescent cell burden and consequently reduces the inflammatory SASP. Individually, D, Q, and F function as senolytic drugs (serving to kill senescent cells).[11,35] F and D+Q improve health span by reducing senescent cell burden.[19,36–38] D+Q has also been shown to alleviate age-related bone loss in mice.[10] Further supporting the merit of potentially conducting a clinical trial of D+Q for radiation-induced bone damage, we recently showed that 11 days after a single oral 3-day course of D+Q, senescent cell abundance was significantly reduced in skin and adipose tissue of patients with diabetic kidney disease.[39] Thus, as in mice, D+Q reduces senescent cell abundance in at least two tissues in humans with a cellular senescence-associated disorder.

To our knowledge, this study is the first comprehensive attempt to use senolytic drugs as stand-alone agents or as a cocktail to alleviate FRT-related bone damage. Although F, D, and Q failed to rescue the FRT-related bone damage as single, stand-alone treatments, the combination D+Q alleviated FRT-induced osteoporosis (Fig. 4). As reported[14,22,40] and as seen in Fig. 6A, with FRT a rapid decrease in mineralization was observed. Osteoblasts that underwent DNA damage,[14] apoptosis (Supplementary Fig. S4),[14,22] or became senescent (Fig. 7E,F), likely failed to deposit substantial mineralized matrix. The extreme reduction in BFR could be a cumulative effect of all three cellular processes. D+Q effectively reduced the number of senescent osteoblasts, with concomitant improvement in BFR. Cumulatively,

reduction of $TIF^+$ osteocytes and osteoblasts by D+Q treatment may have had a direct role in the restoration of bone quality. This was supported by the suppression of *p16*$^{Ink4a}$ and p21 gene expression by D+Q. Static histomorphometry also confirmed that D+Q treatment was able to reverse radiation-induced declines in osteoblasts and osteocytes, as well as effectively suppress the adiposity seen in vehicle-treated radiated bones. These results show a direct correlation between senescence and bone marrow adiposity, one that is supported by other studies that show increased bone marrow adiposity when young MSCs were transplanted in aged mice, known to have a senescent environment.[41]

Accumulation of senescent cells is accompanied by the pro-inflammatory SASP, and its reduction is associated with improved tissue function with aging.[42] We showed that the SASP is prominent at both early (day 14, Fig. 3) and late (day 42, Fig. 8) post-FRT. D+Q treatment effectively minimized the SASP, likely secondary to the clearance of senescent cells. Modulators that can reduce the SASP without elimination of senescent cells,[42] so-called senomorphic agents, might also be effective in preventing radiation-induced bone loss, but likely at the expense of continuous treatment and increased toxicity.

Here we have shown that senescent cells accumulate after FRT, and reduction in senescent cell burden and the related SASP by senolytic drugs alleviates radiation-induced-bone damage. We have provided proof of concept that cellular senescence is a major mechanism underlying osteoporosis related to clinically relevant radiation exposure to bone.

## Supplementary Material

Refer to Web version on PubMed Central for supplementary material.

## Acknowledgments

This work was made possible by Mayo Clinic Clinical and Translational Science Award (CTSA), grant number UL1TR002377, grants from the National Center for Advancing Translational Science (NCATS), a component of the National Institutes of Health (NIH) (to AC and SP) and UL1TR000135 (to DGM and AC), as well as the Robert and Arlene Kogod Professorship (to RJP); P01 AG062413 (SK, JLK, TT, JNF, RJP), P01 AG004875 (SK/DGM), R01 AG048792 (SK/DGM), R01 AR068275 (DGM), K01 AR070241 (JNF), R01 AG 013925 (JLK), the Connor Group (JLK), and the Noaber Foundation (JLK). JFP and AL would like to thank the Ted Nash Foundation.

## References

1. Kirkland JL, Tchkonia T. Cellular senescence: a translational perspective. EBioMedicine. 2017;21:21–8. [PubMed: 28416161]
2. Ozcan S, Alessio N, Acar MB, et al. Unbiased analysis of senescence associated secretory phenotype (SASP) to identify common components following different genotoxic stresses. Aging (Albany NY). 2016;8(7):1316–29. [PubMed: 27288264]
3. Hewitt G, Jurk D, Marques FD, et al. Telomeres are favoured targets of a persistent DNA damage response in ageing and stress-induced senescence. Nat Commun. 2012;3:708. [PubMed: 22426229]
4. Anderson R, Lagnado A, Maggiorani D, et al. Length-independent telomere damage drives post-mitotic cardiomyocyte senescence. EMBO J. 2019;38(5):e100492. [PubMed: 30737259]
5. Fumagalli M, Rossiello F, Clerici M, et al. Telomeric DNA damage is irreparable and causes persistent DNA-damage-response activation. Nat Cell Biol. 2012;14(4):355–65. [PubMed: 22426077]

6. Pereira BI, Devine OP, Vukmanovic-Stejic M, et al. Senescent cells evade immune clearance via HLA-E-mediated NK and CD8(+) T cell inhibition. Nat Commun. 2019;10(1):2387. [PubMed: 31160572]
7. Baker DJ, Wijshake T, Tchkonia T, et al. Clearance of p16Ink4a-positive senescent cells delays ageing-associated disorders. Nature. 2011;479 (7372):232–6. [PubMed: 22048312]
8. Chandra ARA, Pignolo RJ. Osteobiology of aging. 2nd ed. Champaign, IL: Humana Press; 2018 pp 3–37.
9. Farr JN, Fraser DG, Wang H, et al. Identification of senescent cells in the bone microenvironment. J Bone Miner Res. 2016;31(11):1920–9. [PubMed: 27341653]
10. Farr JN, Xu M, Weivoda MM, et al. Targeting cellular senescence prevents age-related bone loss in mice. Nat Med. 2017;23(9):1072–9. [PubMed: 28825716]
11. Zhu Y, Tchkonia T, Pirtskhalava T, et al. The Achilles' heel of senescent cells: from transcriptome to senolytic drugs. Aging Cell. 2015;14(4): 644–58. [PubMed: 25754370]
12. Willey JS, Lloyd SA, Robbins ME, et al. Early increase in osteoclast number in mice after whole-body irradiation with 2 Gy X rays. Radiat Res. 2008;170(3):388–92. [PubMed: 18763868]
13. Chandra A, Lin T, Tribble MB, et al. PTH1–34 alleviates radiotherapy-induced local bone loss by improving osteoblast and osteocyte survival. Bone. 2014;67:33–40. [PubMed: 24998454]
14. Chandra A, Lin T, Young T, et al. Suppression of sclerostin alleviates radiation-induced bone loss by protecting bone-forming cells and their progenitors through distinct mechanisms. J Bone Miner Res. 2017;32(2):360–72. [PubMed: 27635523]
15. So EY, Ouchi T. Decreased DNA repair activity in bone marrow due to low expression of DNA damage repair proteins. Cancer Biol Ther. 2014;15(7):906–10. [PubMed: 24755532]
16. Almeida-Porada G, Rodman C, Kuhlman B, et al. Exposure of the bone marrow microenvironment to simulated solar and galactic cosmic radiation induces biological bystander effects on human hematopoiesis. Stem Cells Dev. 2018;27(18):1237–56. [PubMed: 29698131]
17. Muralidharan S, Sasi SP, Zuriaga MA, et al. Ionizing particle radiation as a modulator of endogenous bone marrow cell reprogramming: implications for hematological cancers. Front Oncol. 2015;5:231. [PubMed: 26528440]
18. Chandra A, Park SS, Pignolo RJ. Potential role of senescence in radiation-induced damage of the aged skeleton. Bone. 2019;120: 423–31. [PubMed: 30543989]
19. Yousefzadeh MJ, Zhu Y, McGowan SJ, et al. Fisetin is a senotherapeutic that extends health and lifespan. EBioMedicine. 2018;36:18–28. [PubMed: 30279143]
20. Bouxsein ML, Boyd SK, Christiansen BA, Guldberg RE, Jepsen KJ, Muller R. Guidelines for assessment of bone microstructure in rodents using micro-computed tomography. J Bone Miner Res. 2010;25(7):1468–86. [PubMed: 20533309]
21. Schindelin J, Arganda-Carreras I, Frise E, et al. Fiji: an open-source platform for biological-image analysis. Nat Methods. 2012;9(7): 676–82. [PubMed: 22743772]
22. Chandra A, Wang L, Young T, et al. Proteasome inhibitor bortezomib is a novel therapeutic agent for focal radiation-induced osteoporosis. FASEB J. 2018;32(1):52–62. [PubMed: 28860152]
23. Dempster DW, Compston JE, Drezner MK, et al. Standardized nomenclature, symbols, and units for bone histomorphometry: a 2012 update of the report of the ASBMR histomorphometry nomenclature committee. J Bone Miner Res. 2013;28(1):2–17. [PubMed: 23197339]
24. Coppe JP, Desprez PY, Krtolica A, Campisi J. The senescence-associated secretory phenotype: the dark side of tumor suppression. Annu Rev Pathol. 2010;5:99–118. [PubMed: 20078217]
25. Coppe JP, Patil CK, Rodier F, et al. A human-like senescence-associated secretory phenotype is conserved in mouse cells dependent on physiological oxygen. PLoS One. 2010;5(2):e9188. [PubMed: 20169192]
26. Coppe JP, Patil CK, Rodier F, et al. Senescence-associated secretory phenotypes reveal cell-nonautonomous functions of oncogenic RAS and the p53 tumor suppressor. PLoS Biol. 2008;6(12):2853–68. [PubMed: 19053174]
27. Hamilton SA, Pecaut MJ, Gridley DS, et al. A murine model for bone loss from therapeutic and space-relevant sources of radiation. J Appl Physiol (1985). 2006;101(3):789–93. [PubMed: 16741258]

28. Wright LE, Buijs JT, Kim HS, et al. Single-limb irradiation induces local and systemic bone loss in a murine model. J Bone Miner Res. 2015;30 (7):1268–79. [PubMed: 25588731]
29. Oest ME, Franken V, Kuchera T, Strauss J, Damron TA. Long-term loss of osteoclasts and unopposed cortical mineral apposition following limited field irradiation. J Orthop Res. 2015;33(3):334–42. [PubMed: 25408493]
30. Scheven BA, Wassenaar AM, Kawilarang-de Haas EW, Nijweide PJ. Comparison of direct and indirect radiation effects on osteoclast formation from progenitor cells derived from different hemopoietic sources. Radiat Res. 1987;111(1):107–18. [PubMed: 3602348]
31. Scheven BA, Wassenaar AM, Kawilarang-de Haas EW, Nijweide PJ. Direct and indirect radiation effects on osteoclast formation in vitro. Bone Miner. 1987;2(4):291–300. [PubMed: 3505764]
32. Wang H, Chen Q, Lee SH, Choi Y, Johnson FB, Pignolo RJ. Impairment of osteoblast differentiation due to proliferation-independent telomere dysfunction in mouse models of accelerated aging. Aging Cell. 2012;11(4):704–13. [PubMed: 22621437]
33. Wang Y, Schulte BA, Zhou D. Hematopoietic stem cell senescence and long-term bone marrow injury. Cell Cycle. 2006;5(1):35–8. [PubMed: 16319536]
34. Rodrigues-Moreira S, Moreno SG, Ghinatti G, et al. Low-dose irradiation promotes persistent oxidative stress and decreases self-renewal in hematopoietic stem cells. Cell Rep. 2017;20(13):3199–211. [PubMed: 28954235]
35. Zhu Y, Doornebal EJ, Pirtskhalava T, et al. New agents that target senescent cells: the flavone, fisetin, and the BCL-XL inhibitors, A1331852 and A1155463. Aging (Albany NY). 2017;9(3):955–63. [PubMed: 28273655]
36. Xu M, Pirtskhalava T, Farr JN, et al. Senolytics improve physical function and increase lifespan in old age. Nat Med. 2018;24(8):1246–56. [PubMed: 29988130]
37. Schafer MJ, Miller JD, LeBrasseur NK. Cellular senescence: implications for metabolic disease. Mol Cell Endocrinol. 2017;455:93–102. [PubMed: 27591120]
38. Roos CM, Zhang B, Palmer AK, et al. Chronic senolytic treatment alleviates established vasomotor dysfunction in aged or atherosclerotic mice. Aging Cell. 2016;15(5):973–7. [PubMed: 26864908]
39. Hickson LJ, Langhi Prata LGP, Bobart SA, et al. Senolytics decrease senescent cells in humans: preliminary report from a clinical trial of Dasatinib plus Quercetin in individuals with diabetic kidney disease. EBioMedicine. 2019;47:446–56. [PubMed: 31542391]
40. Chandra A, Lin T, Zhu J, et al. PTH1–34 blocks radiation-induced osteoblast apoptosis by enhancing DNA repair through canonical Wnt pathway. J Biol Chem. 2015;290(1):157–67. [PubMed: 25336648]
41. Singh L, Brennan TA, Russell E, et al. Aging alters bone-fat reciprocity by shifting in vivo mesenchymal precursor cell fate towards an adipogenic lineage. Bone. 2016;85:29–36. [PubMed: 26805026]
42. Xu M, Tchkonia T, Ding H, et al. JAK inhibition alleviates the cellular senescence-associated secretory phenotype and frailty in old age. Proc Natl Acad Sci U S A. 2015;112(46):E6301–10. [PubMed: 26578790]

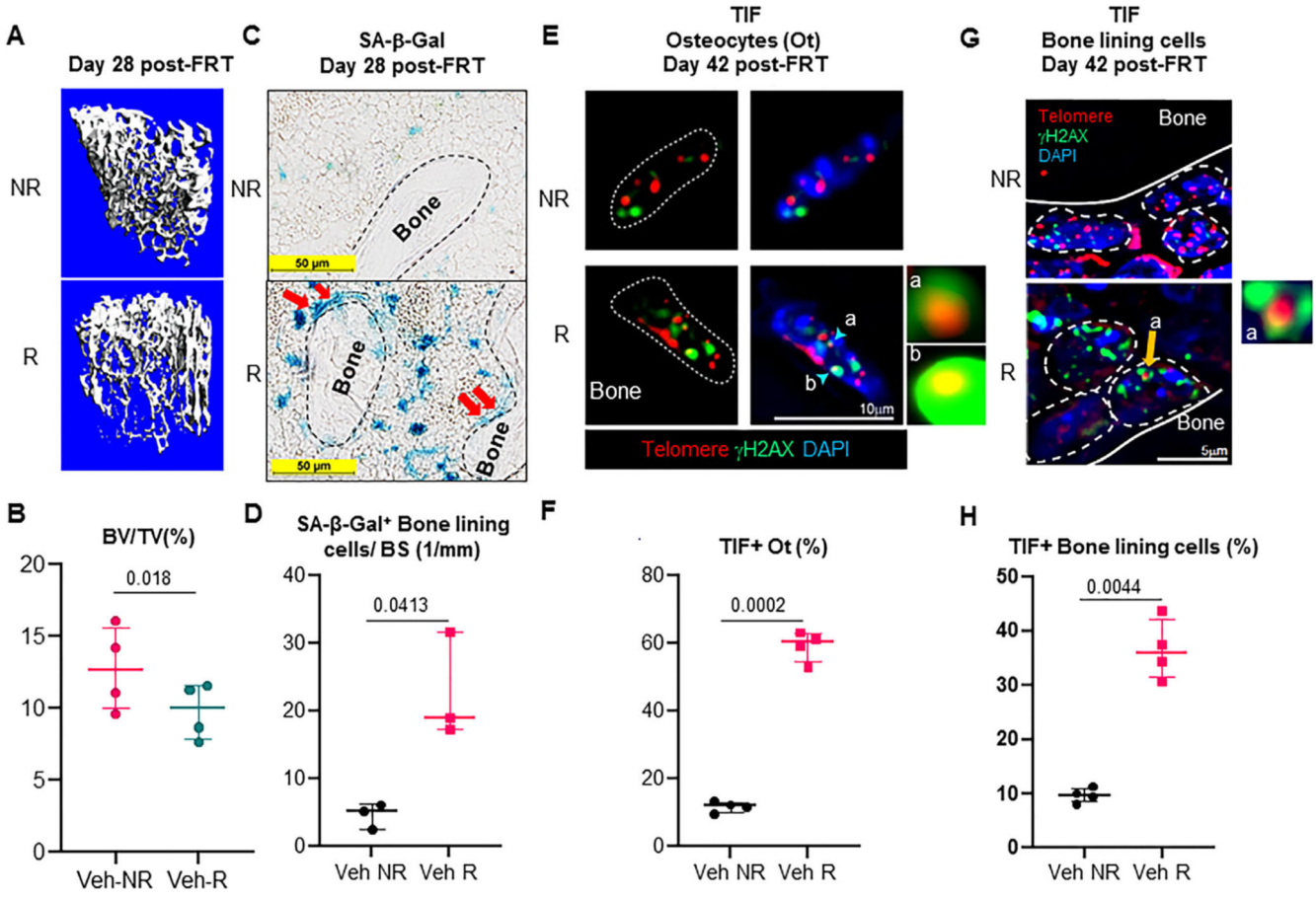


**Fig. 1.**

Identification of senescent osteoblasts and osteocytes in radiated bones. (*A*,*B*) The right legs of C57BL/6 mice were radiated (24 Gy) in a 5-mm region near the femoral metaphysis, while the left leg served as control. R and NR femurs at 28 days post-FRT were harvested, μCT scanned ($n = 4$ animals), fixed, decalcified, and processed for frozen sectioning. Representative 3D-reconstructed images are shown in *A*; BV/TV is shown in *B*. (*C*) SA-β-gal staining shows the presence of senescent osteoblasts (red arrows) in frozen femur sections ($n = 3$ animals) at 28 days post-FRT. (*D*) Quantification of SA-β-gal$^+$ cells lining the bone surface. (*E*) R and NR femurs ($n = 4$ animals) at 42 days post-FRT were harvested and processed for MMA embedding. Five-micrometer (5-μm) deplasticized sections were processed for TIF staining and TIFs were detected. Telomeres (red) and γH2AX (green) are shown in Ot of nondecalcified NR and R femurs, 42 days post-FRT. The co-localization detects yellow-orange TIF foci. Insets "a" and "b" show images representative of TIF$^+$ (R) osteocyte nuclei. (*F*) Quantification of TIF$^+$ osteocytes from NR and R femurs. (*G*) Detection of TIF$^+$ bone lining cells including osteoblasts in nondecalcified NR and R femurs, 42 days post-FRT. Inset "a" shows a representative image of a TIF from an osteoblast. (*H*) Quantification of TIF$^+$ bone lining cells on the trabecular bone surface in NR and R femurs. Statistical analysis was done using GraphPad Prism and *p* value was calculated using a two-tailed paired *t* test to compare the R and NR bones from the same animals. BV/TV = bone volume fraction of the total volume; Ot = osteocytes.

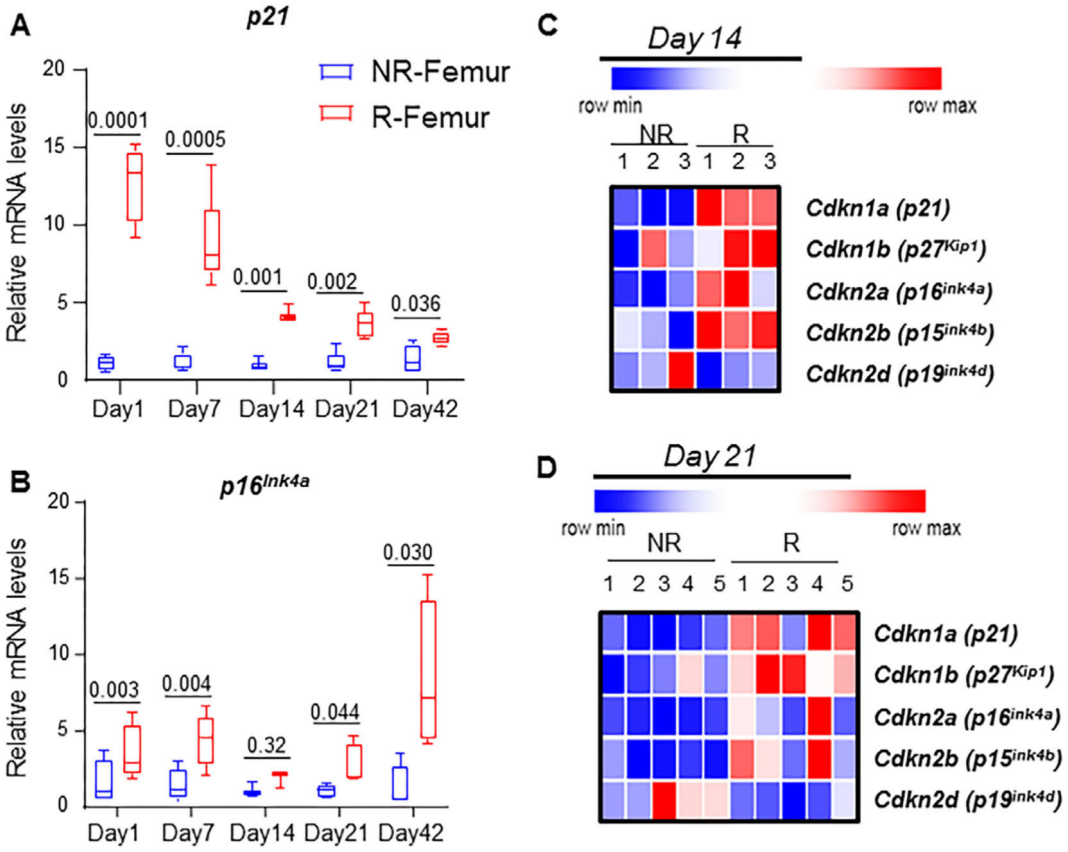


**Fig. 2.**

Focal radiation induces markers of senescence in bone. NR and R femurs were collected on days 1, 7, 14, 21, and 42, and qRT-PCR was performed to detect *p21* (*A*) and $p16^{Ink4a}$ (*B*). (*C*,*D*) Heat maps of CDKi genes were determined by RT-qPCR from NR and R femurs collected 14 days (*C*, $n = 3$ mice) and 21 days (*D*, $n = 5$mice) post-FRT. Statistical analysis was done using GraphPad Prism and *p* value was calculated using a two-tailed paired *t* test to compare the R and NR bones from the same animals.

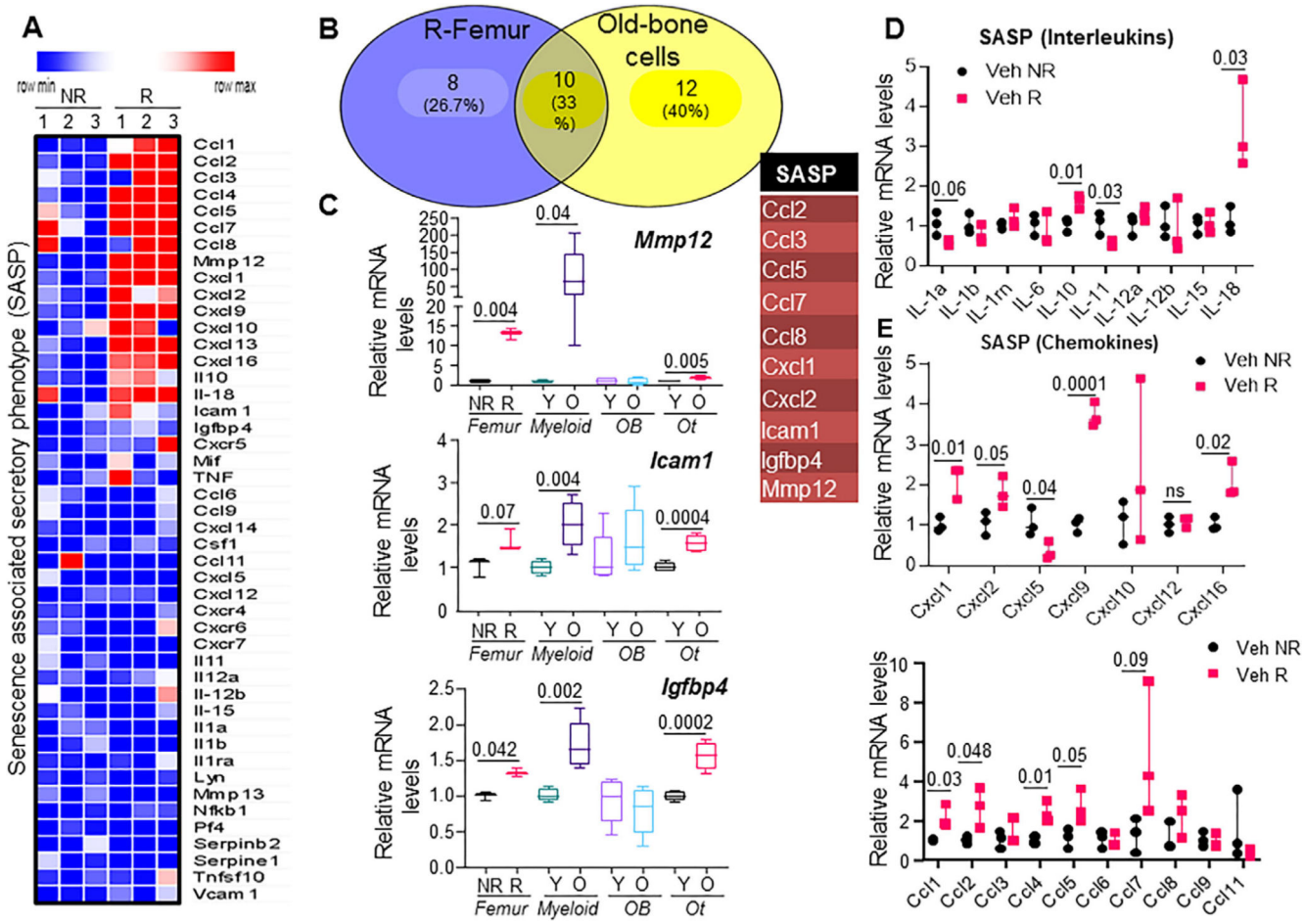


**Fig. 3.**

Radiation of bone induces a SASP similar to that of aged bone cells. (*A*) Heat map of SASP genes from NR and R femurs ($n = 3$ mice) at 14 days post-FRT. (*B*) Venn diagram representing SASP genes that were commonly expressed between R femurs from 4-month-old male mice and old bone cells from 24-month old male mice (table). (*C*) Comparison of expression levels of SASP genes Mmp12, Icam1, and Igfbp4, between R bones and NR bones at 14 days post-FRT, with enriched cell populations from bones of young (Y) versus old (O) animals. *y* axis: fold change normalized against NR (for comparison between NR versus R), and normalized against Y (for comparison between Y versus O). Expression of SASP genes that are classified as interleukins and chemokines are shown (*D* and *E*, respectively). *y* axis: fold change normalized against NR (for comparison between NR versus R). Statistical analysis was done using GraphPad Prism and *p* value was calculated using a two-tailed paired *t* test to compare the R and NR bones from the same animals, and using a two-sampled *t* test for comparison of young and old bone cells.

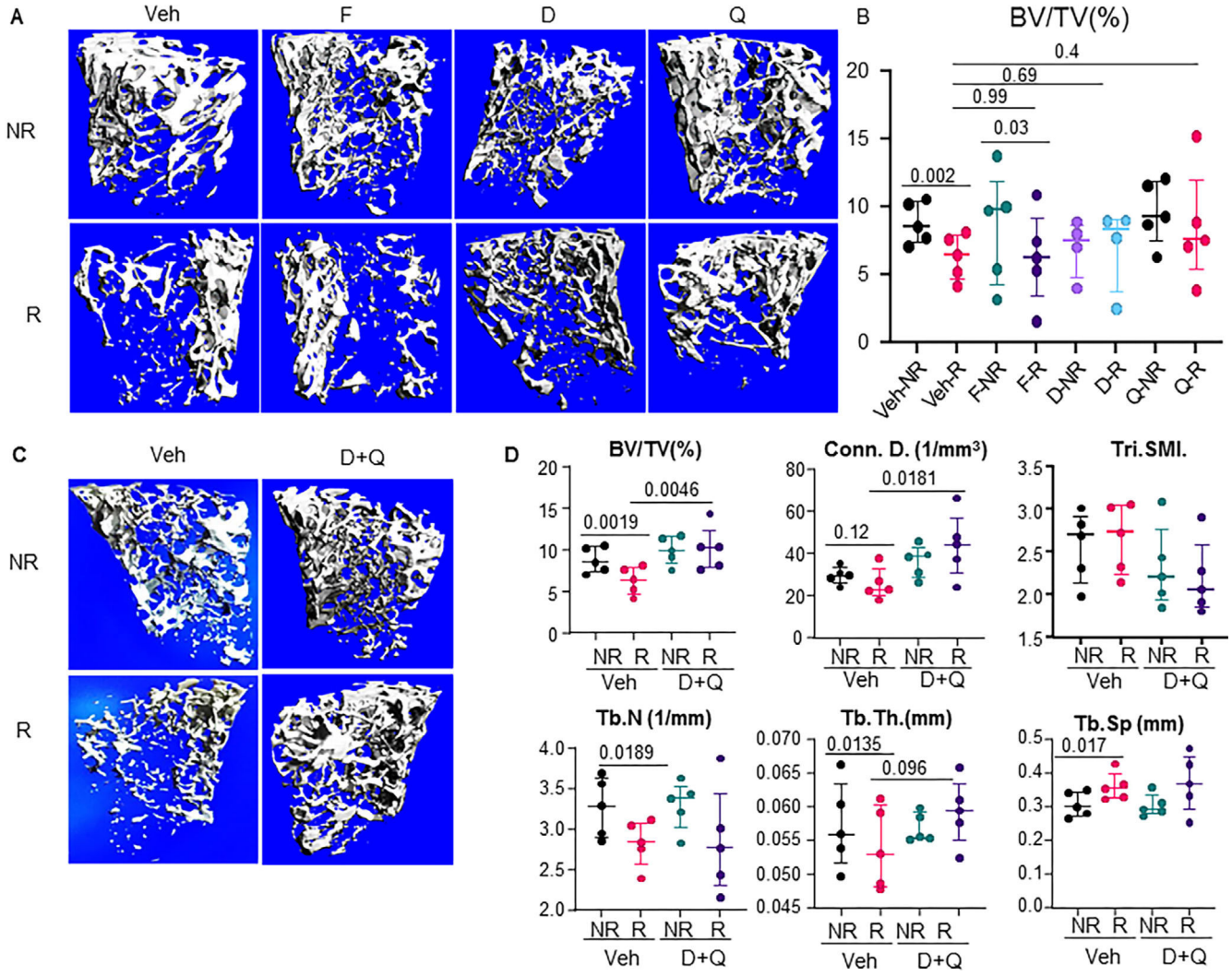


**Fig. 4.**

Targeted clearance of senescent cells alleviates radiation-induced bone damage. Four-month-old C57BL/6 male mice received radiation (24 Gy) in a 5-mm region of the right femoral metaphysis, accompanied with intermittent treatments on days 0 and 14, with either vehicle ($n = 5$ mice) or senolytic drug treatment (F: fisetin, 50 mg/kg, $n = 5$ mice; D: dasatinib, 5 mg/kg, $n = 4$ mice; Q: quercetin, 50 mg/kg, $n = 5$ mice) or a cocktail of D+Q (5 mg/kg D and 50 mg/kg Q, $n = 5$ mice); bones were collected on day 42 post-FRT. (*A*) Images represent 3D representations of the bone architecture generated by ex vivo μCT scans using Viva40. (*B*) Percentage of bone volume over total volume. (*C*) Experiment was performed as described in *A*. 3D representation of μCT data of vehicle ($n = 5$) and D+Q ($n = 5$). (*D*) Bone architecture parameters for vehicle-treated and D+Q-treated NR and R femurs. Statistical analyses were done using GraphPad Prism and *p* values were calculated using a two-way ANOVA with a Tukey post hoc analysis.

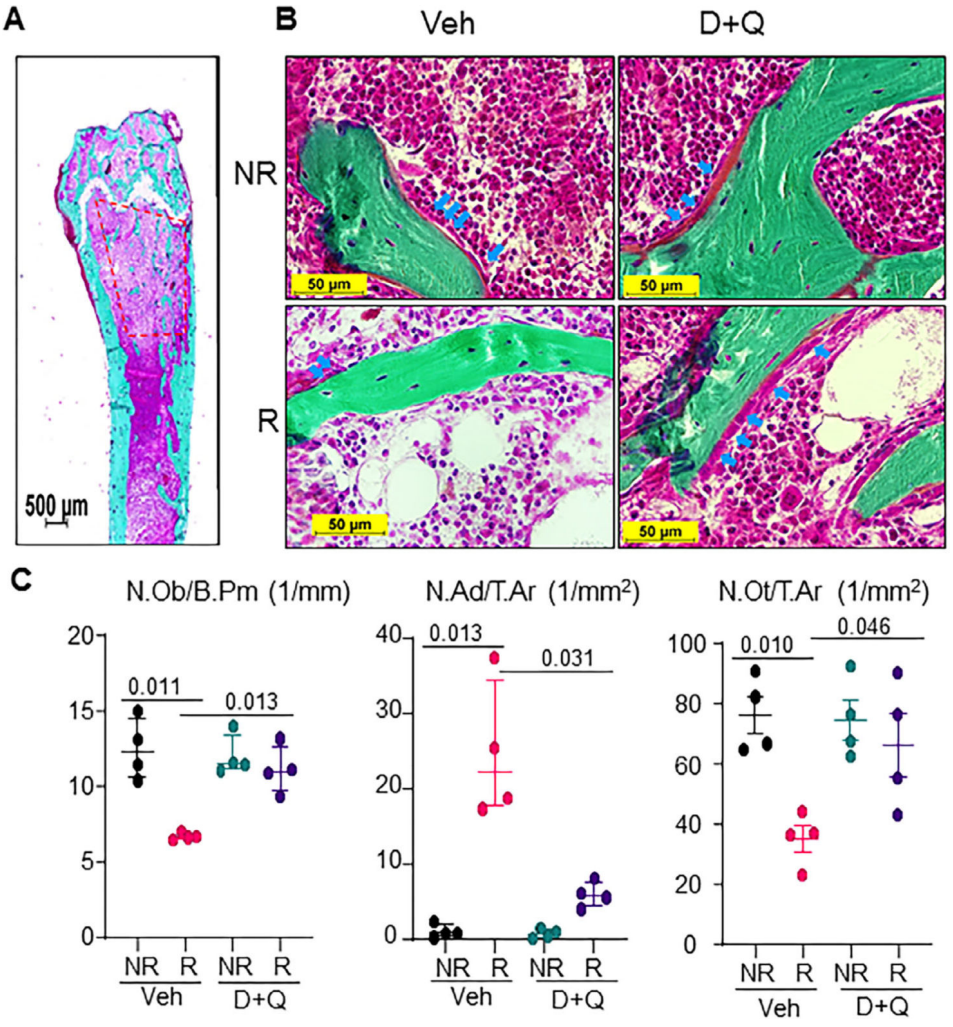


**Fig. 5.**

D+Q preserves functional osteoblasts and restores bone formation in radiated femurs. Four-month-old C57BL/6 male mice received radiation (24 Gy) in a 5-mm region of the right femoral metaphysis, accompanied with intermittent treatments on days 0 and 14, with either vehicle ($n = 4$ mice) or D+Q (5 mg/kg D and 50 mg/kg Q, $n = 4$ mice); bones were collected on day 42 post-FRT and processed for MMA embedding. (*A*) A representative Goldner's Trichrome–stained bone section showing the region of interest (1–4 mm below the growth plate) used for static histomorphometry. (*B*) Representative images from vehicle-treated and D+Q-treated NR and R femurs (arrows indicate osteoblasts). (*C*) Quantification for N.Ob per mm of bone surface N. Ad per $mm^2$ of total area, and total N.Ot per $mm^2$ of total area. Results are expressed as medians with interquartile range. Statistical analyses were done using GraphPad Prism and *p* values were calculated using a two-way ANOVA ($\alpha = 0.05$) with a Tukey post hoc analysis. N.Ad = number of adipocytes; N.Ob = number of osteoblasts; N.Ot = number of osteocytes.

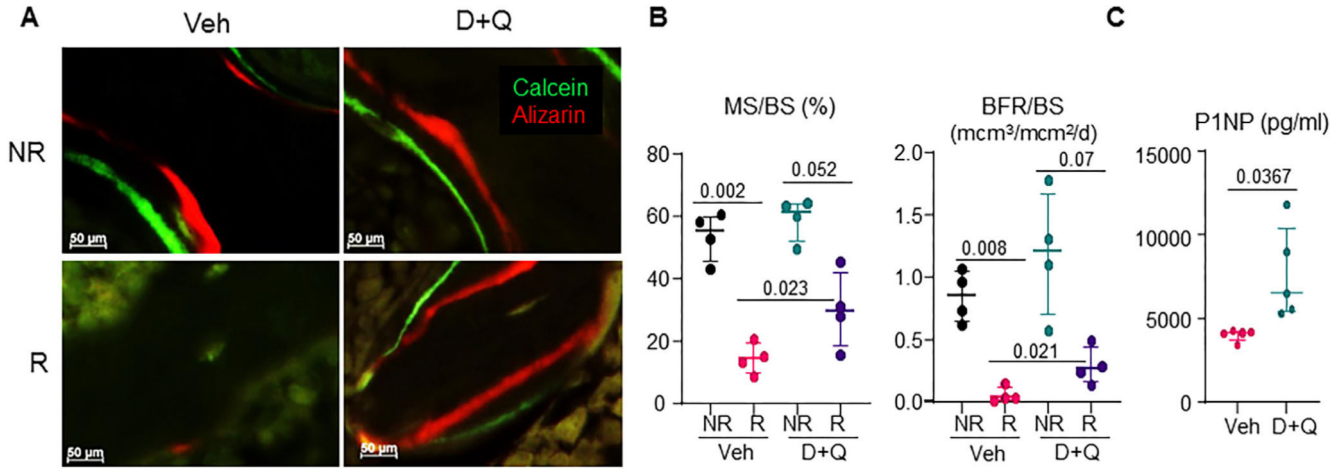


**Fig. 6.**

D+Q preserves bone formation in radiated femurs. Four-month-old C57BL/6 male mice received radiation (24 Gy) in a 5-mm region of the right femoral metaphysis, accompanied by intermittent treatments on days 0 and 14, with either vehicle ($n = 4$ mice) or D+Q (5 mg/kg D and 50 mg/kg Q, $n = 4$ mice); bones were collected on day 42 post-FRT and processed for MMA embedding. (*A*) Animals were injected with Alizarin and Calcein on days 9 and 2, respectively, before bones were harvested for MMA embedding. Unstained 8-μm MMA sections were used to visualize Alizarin (red) and Calcein (green) fluorescence. (*B*) MS/BS and BFR/BS were quantified. (*C*) Serum protein measurement of P1NP from vehicle-treated and D+Q-treated animals ($n = 5$/group) by ELISA. Results are expressed as medians with interquartile range. Statistical analyses were done using GraphPad Prism and $p$ values were calculated using a two-way ANOVA ($\alpha = 0.05$) with a Tukey post hoc analysis. BFR/BS = bone formation rate per bone surface; MS/BS = mineralizing surface per bone surface.

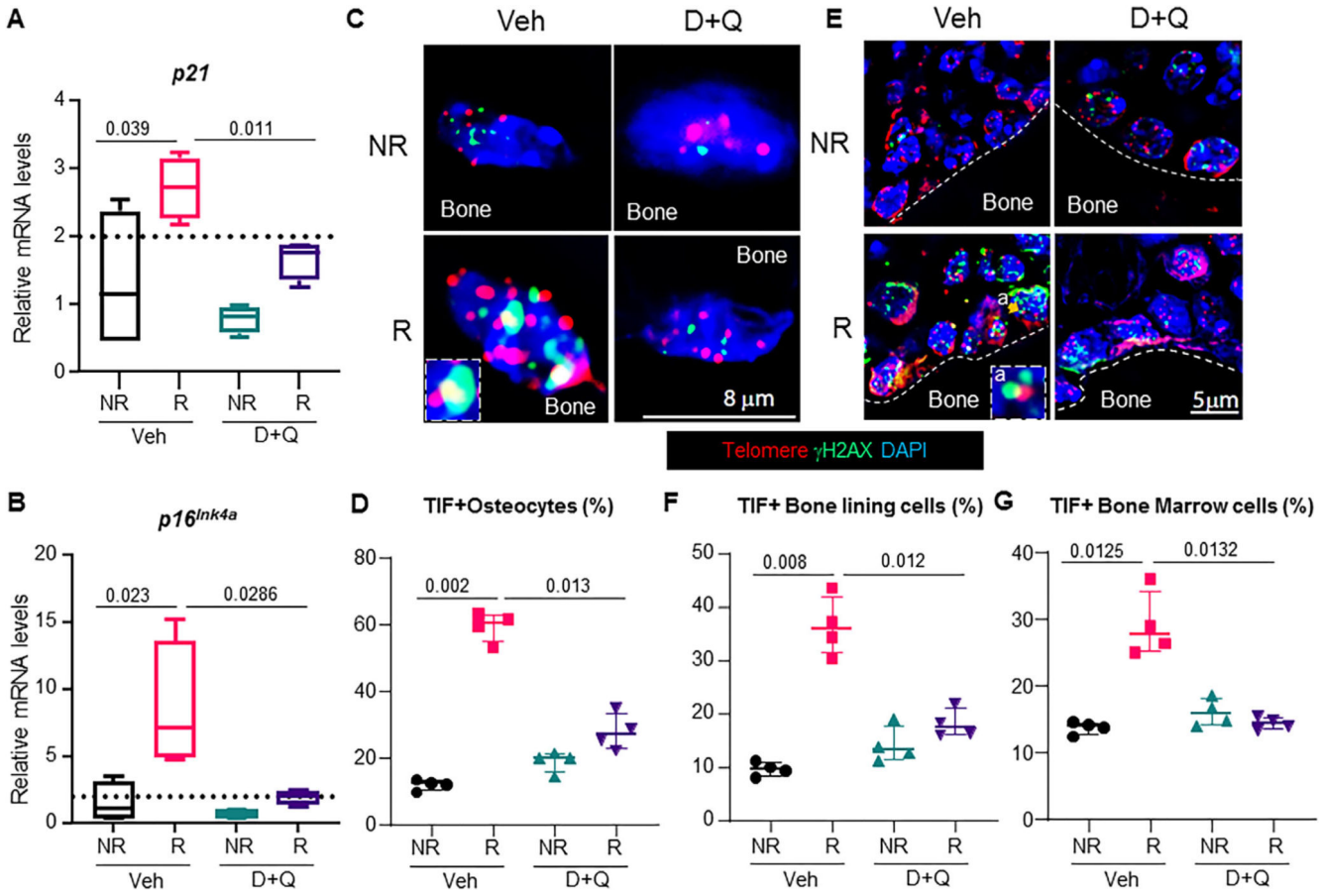


**Fig. 7.**

The senolytic cocktail, D+Q, reduces the senescent cell burden in radiated bones. Four-month-old C57BL/6 male mice received radiation (24 Gy) in a 5-mm region of the right femoral metaphysis, accompanied with intermittent treatments on days 0 and 14, with either vehicle ($n$ = 8 mice) or D+Q (5 mg/kg D and 50 mg/kg Q, $n$ = 8 mice); bones were collected on day 42 post-FRT and processed for mRNA ($n$ = 4/group) or histology ($n$ = 4/group). Gene expression levels of *p21* (*A*) and *p16*$^{Ink4a}$ (*B*) were detected by qRT-PCR in NR-femurs and R-femurs 42 days post-FRT. (*C*) Representative images showing the co-localization of telomere foci with γH2AX in osteocytes (inset in Veh-R panel is a TIF+ osteocyte). (*D*) TIF+ osteocytes (from $n$ = 4 animals/group) were quantified by visualizing the co-localization of telomere foci (red) and γH2AX (green). TIFs were scored by overlapping staining (yellow). (*E*) TIF$^{+}$ bone lining cells including osteoblasts were scored as cells on the trabecular bone surface with co-localization of telomere foci and γH2AX (inset in Veh-R panel is a TIF$^{+}$ osteoblast). (*F*) Quantification of TIF$^{+}$ bone lining cells including osteoblasts (from $n$ = 4 animals/group) on the bone surface. (*G*) Quantification of TIF$^{+}$ bone marrow cells (from $n$ = 4 animals/ group). Results are expressed as medians with interquartile range. Statistical analyses were done using GraphPad Prism and $p$ values were calculated using a two-way ANOVA (α = 0.05) with a Tukey post hoc analysis.

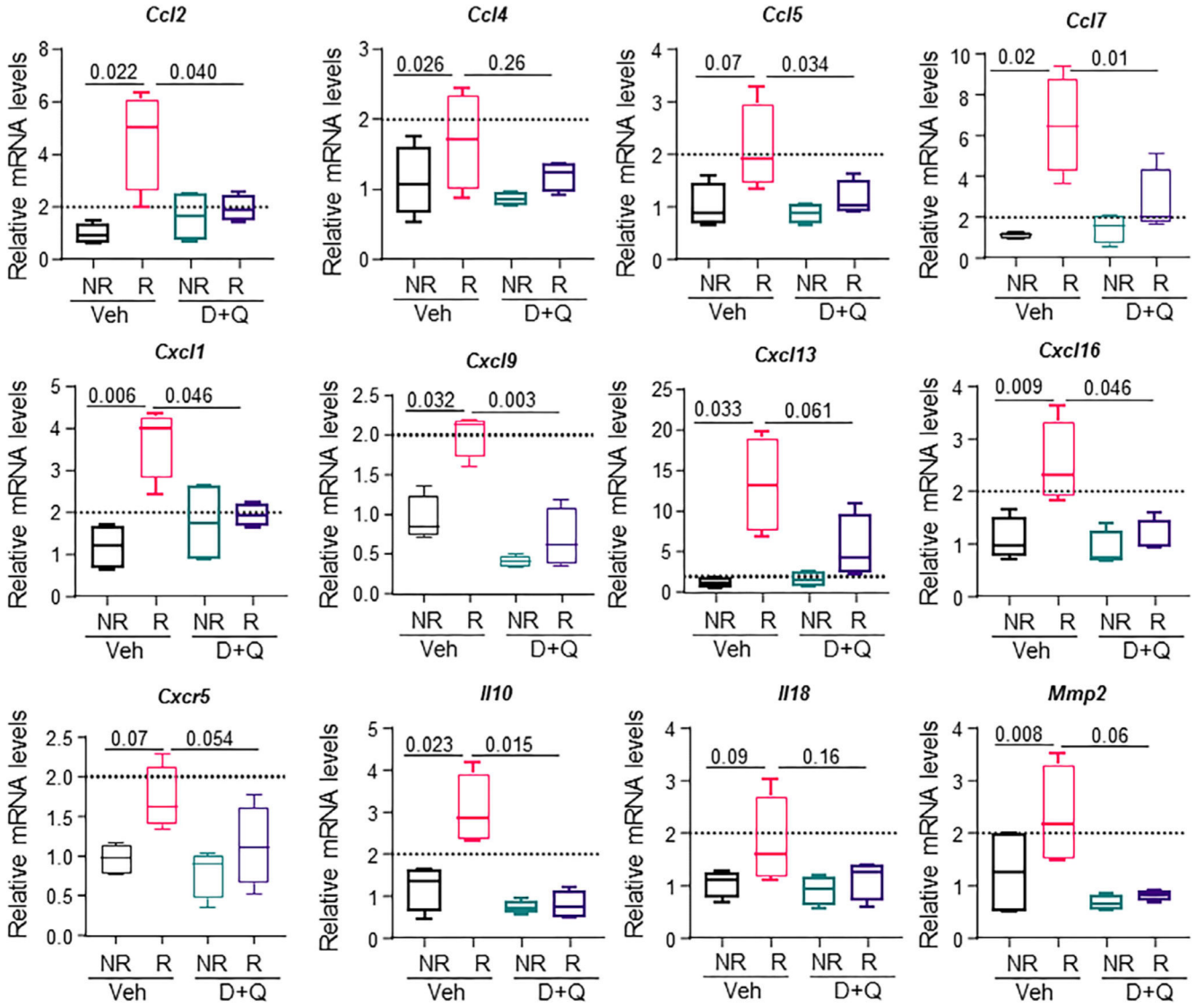


**Fig. 8.**

Clearance of senescent cells by D+Q reduces the SASP in radiated bones. Four-month old C57BL/6 male mice received radiation (24 Gy) in a 5-mm region of the right femoral metaphysis, accompanied with intermittent treatments on day 0 and 14, with either vehicle ($n$ = 4 mice) or D+Q (5 mg/kg D and 50 mg/kg Q, $n$ = 4 mice). Bones were collected on day 42 post-FRT and processed for mRNA analysis. Gene expression levels for 12 SASP factors at 42 days post-FRT from vehicle-treated and D+Q–treated NR femurs and R femurs are presented. Results are expressed as medians with interquartile range. Statistical analyses were done using GraphPad Prism and $p$ values were calculated using a two-way ANOVA ($\alpha$ = 0.05) with a Tukey post hoc analysis.